SYNAPSE 67:489–501 (2013)

Studies of the Metabotropic Glutamate Receptor 5 Radioligand [^{11}C]ABP688 With *N*-Acetylcysteine Challenge in Rhesus Monkeys

CHRISTINE M. SANDIEGO,[1,2*] NABEEL NABULSI,[2] SHU-FEI LIN,[2] DAVID LABAREE,[2] SOHEILA NAJAFZADEH,[2] YIYUN HUANG,[2] KELLY COSGROVE,[2,3] AND RICHARD E. CARSON[1,2]

[1]*Department of Biomedical Engineering, Yale University, New Haven, Connecticut 06520*
[2]*PET Center, Diagnostic Radiology, Yale University, New Haven, Connecticut 06520*
[3]*Department of Psychiatry, Yale University, New Haven, Connecticut 06520*

KEY WORDS PET; mGluR5 radioligand; NAC; allosteric modulator; test-retest; nonhuman primate

ABSTRACT Detecting changes in receptor binding at the metabotropic glutamate receptor 5 (mGluR5) with the PET allosteric antagonist, [^{11}C]ABP688, may be valuable for studying dysfunctional glutamate transmission associated with psychiatric illnesses. This study was designed to validate the findings of a recent pilot study in baboons which reported a significant global decrease from baseline [^{11}C]ABP688 binding after increasing endogenous glutamate with 50 mg/kg *N*-acetylcysteine (NAC), with no change from test to retest. In rhesus monkeys ($n = 5$), paired [^{11}C]ABP688 scans were performed on the same day on the Focus-220 as follows ($n = 3$ per group): test-retest, baseline-NAC (50 mg/kg), and baseline-NAC (100 mg/kg). Multiple modeling methods were evaluated for kinetic analysis to estimate the total volume of distribution (V_T) and non-displaceable binding potential (BP_{ND}) in regions-of-interest (ROIs), with the cerebellum gray matter (CGM) as the reference region. There was an increasing trend from test to retest BP_{ND} across ROIs (13%). NAC (50 mg/kg and 100 mg/kg) increased V_T (5% and 19%) and decreased BP_{ND} (3% and 10%), respectively, significant only for V_T in ROIs at the 100 mg/kg dose. High intersubject variability in BP_{ND} was comparable to that reported in the baboon study. However, interpretability of BP_{ND} is difficult with increases in V_T in the CGM reference region at the higher NAC dose. Additionally, the net reduction in BP_{ND} from the baseline-NAC scans may be obscured due to observed increases in test-retest BP_{ND}. Thus, we did not strictly replicate the findings in the baboon study based on BP_{ND}. **Synapse 67:489–501, 2013.** © 2013 Wiley Periodicals, Inc.

INTRODUCTION

Receptor radioligands are useful for measuring the dynamics of various neurotransmitters with positron emission tomography (PET), especially in the dopamine system (Laruelle, 2000; Shen et al., 2012). Recently, there has been great interest in the development of PET imaging probes to target the glutamate system. The ability to measure alterations in glutamate neurotransmission in vivo with PET is valuable for elucidating the underlying mechanisms that give rise to central nervous system (CNS) disorders such as schizophrenia, anxiety, and drug addiction.

Glutamate is the main excitatory neurotransmitter in the CNS where its effects are mediated at glutamate receptors either at ionotropic receptors via ligand gated channels, or at metabotropic receptors via activation of G-protein coupled second messengers (Kew and Kemp, 2005). Ionotropic glutamate

Additional Supporting Information may be found in the online version of this article.

Contract grant sponsor: Training grant; Contract grant number: 1-T90-DK070068; Contract grant sponsor: CTSA; Contract grant number: UL1 RR024139; Contract grant sponsors: National Center for Advancing Translational Science (NCATS), National Institutes of Health (NIH), NIH roadmap for Medical Research.

*Correspondence to: Christine M. Sandiego, PET Center, Yale School of Medicine, P.O. Box 208048, New Haven, CT 06520-8048, USA. E-mail: christine.sandiego@yale.edu

Received 11 December 2012; Accepted 12 February 2013

DOI: 10.1002/syn.21656

Published online 20 February 2013 in Wiley Online Library (wileyonlinelibrary.com).

© 2013 WILEY PERIODICALS, INC.

receptors (iGluRs) produce fast-acting excitatory effects (e.g., α-amino-3-hydroxyl-5-methyl-4-isoxazole-propionate (AMPA), kainate, and N-methyl-D-aspartate (NMDA)). Conversely, metabotropic glutamate receptors (mGluRs) play a modulatory role to fine-tune the timing and magnitude of glutamate transmission and are classified into three groups based on structure and function: Group I (subtypes 1 and 5), Group II (subtypes 2 and 3), and Group III (subtypes 4, 6, 7, and 8) (Cosgrove et al., 2011; Spooren et al., 2003). Groups II and III mGluRs are mainly located pre-synaptically to regulate neurotransmitter release, whereas group I mGluRs are mostly localized post-synaptically to modulate iGluR excitability (O'Brien et al., 2003).

Metabotropic glutamate subtype 5 receptors (mGluR5) contain both orthosteric and allosteric binding sites and are tightly coupled to NMDA iGluR function (Kew and Kemp, 2005; Perroy et al., 2008). Thus, allosteric modulators at mGluR5 are targets for therapy and treatment for a myriad of neuropsychiatric illnesses. Positive allosteric modulators (PAM), or potentiators, exert agonist effects at mGluR5 to indirectly stimulate NMDA receptor hypofunction to alleviate cognitive symptoms associated with schizophrenia and drug use (Cleva and Olive, 2011; de Bartolomeis et al., 2012). Negative allosteric modulators (NAM) are antagonists at mGluR5 with implications for treatment of Fragile X syndrome (Michalon et al., 2012; Sokol et al., 2011), depression (Deschwanden et al., 2011; Liu et al., 2012), anxiety (Riaza Bermudo-Soriano et al., 2012), and addiction (Carroll, 2008; Cleva et al., 2010).

The PET radiotracer, [^{11}C]ABP688 (3-(6-methylpyridin-2-ylethynyl)-cyclohex-2-enone-*O*-[11]C-methyloxime), is a non-competitive antagonist at the mGluR5 allosteric site (Ametamey et al., 2006; Hintermann et al., 2007). In baboons, binding specificity of [^{11}C]ABP688 to mGluR5 was shown after direct blockade with NAM, 3-((2-methyl-1,3-thiazol-4-yl) ethynyl)pyridine (MTEP, 1 mg/kg), estimated at about 90% occupancy via the Lassen graphical approach (DeLorenzo et al., 2011b). The smallest change in V_T (7%) post-MTEP was observed in the cerebellum gray matter (CGM), suggesting its use as a possible reference region. A recent pilot study in baboons showed that it may be possible to detect acute fluctuations in endogenous glutamate at mGluR5, reporting a significant global reduction of ~17% in [^{11}C]ABP688 BP_{ND} following the administration of *N*-acetylcysteine (NAC), a facilitator of glutamate release (Miyake et al., 2011). In addition, test-retest studies were performed where no change in [^{11}C]ABP688 binding was observed. Miyake et al., proposed that the NAC-induced increase in glutamate produced an affinity shift for [^{11}C]ABP688 at the mGluR5 allosteric site. However, due to the small study size ($n = 3$), further studies were needed to validate this finding.

The aim of this study was to replicate and extend the findings of the baboon study (Miyake et al., 2011) in rhesus monkeys with [^{11}C]ABP688 test-retest studies and a pharmacological challenge with NAC (50 mg/kg). A higher dose of NAC (100 mg/kg) was also added. We hypothesized that increasing endogenous glutamate with NAC would decrease [^{11}C]ABP688 binding in a dose-dependent manner. Rhesus monkeys were used based on availability and inability to properly position the baboon head in the Focus-220 small animal scanner. Since there are no published modeling studies for [^{11}C]ABP688 in rhesus monkeys, different modeling approaches were evaluated and used for the analysis of [^{11}C]ABP688 PET data.

MATERIALS AND METHODS

Study design

PET scans were performed on the Focus-220 small animal scanner (full-width-at-half-maximum (FWHM) resolution ~1.5 mm) (Siemens/CTI, Knoxville, TN) in five rhesus monkeys (one female, four males, mean weight: 10.4 ± 4.4 kg) under a protocol approved by the Institutional Animal Care and Use Committee. Paired bolus [^{11}C]ABP688 scans were performed as follows: test-retest ($n = 3$), baseline-NAC (50 mg/kg, labeled NAC 1) ($n = 3$), and baseline-NAC (100 mg/kg, labeled NAC 2) ($n = 3$). Injections were ~3 h apart, and [^{11}C]ABP688 scans were performed on the same day. For one pair, however, the baseline and NAC 1 scans were performed on separate days. [^{11}C]ABP688 was administered as a 3-min bolus in eight of nine sets of scans; the tracer was administered as a bolus plus constant infusion (B/I, $K_{bol} = 60$ min) in one pair of scans from the baseline-NAC 1 group (Carson et al., 1993). Since modeling methods were used in all cases, bolus and B/I studies were analyzed together.

The general study design is shown in Figure 1. Animals were initially anesthetized ketamine hydrochloride (10 mg/kg, IM), then transported to the PET facility 2 h prior to the initial [^{11}C]ABP688 injection. Once intubated, the animals were maintained on oxygen and isoflurane (~1.5%) throughout the study. A 9-min transmission scan preceded each of the emission scans. [^{11}C]ABP688 was administered and emission data were collected for 90 min, where the first acquisition was the test or baseline scan (Fig. 1A). Mass and dose values are summarized in Table I. For the challenge scan, NAC (50 mg/kg or 100 mg/kg; Alfa Aesar #A15409, dissolved in 0.9% saline) was infused for 60 min, beginning 1 h prior to the second [^{11}C]ABP688 injection followed by another 90 min acquisition, similar to the Miyake et al. (2011) study (Fig. 1B).

Our study was designed to closely match the parameters of the baboon study, where no apparent differences between injected dose, injected mass, and specific activity were observed. However, there may

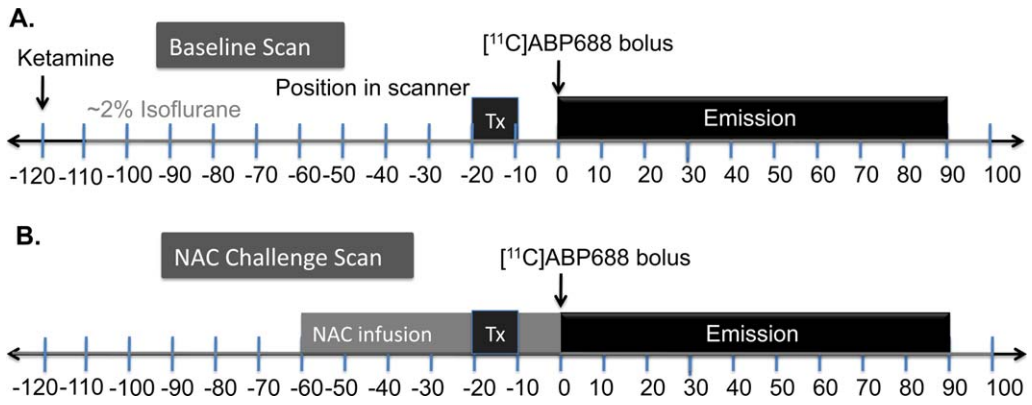

Fig. 1. [^{11}C]ABP688 and NAC challenge study design, each using paired bolus scans performed on the same day, with ~3 h interval between scans. A 9-min transmission (Tx) scan preceded each 90-min emission acquisition. **A**: For the baseline scan, monkeys were induced with ketamine 2 h prior to tracer injection and maintained on isoflurane for the duration of the scans. **B**: For the challenge scan, NAC (50 mg/kg or 100 mg/kg) was infused over 60 min, beginning 1 h prior to the second [^{11}C]ABP688 injection. Depending on the timing of radiosynthesis, the time difference between the end of the first scan and beginning of the second [^{11}C]ABP688 injection varied between 1–3 h.

have been differences in total scan day duration for paired bolus studies ranging from 4 to 6 h, depending on radiosynthesis timing.

Radiochemistry

Reagents and solvents were purchased from commercial suppliers and used without purification. ABP688 standard and the desmethyl precursor were obtained from the NYPSI/Columbia University Medical Center. The radiotracer was synthesized using the loop method, by reacting the desmethyl-ABP688 precursor (~0.5 mg) with [^{11}C]methyl iodide in anhydrous dimethylformamide (0.1 mL) in the presence of base. The crude product was purified by reverse phase semi-preparative high-performance liquid chromatography (HPLC) (Jones Genesis C18 column, 4 μm, 10 × 250 mm; mobile phase: acetonitrile: 0.1 M ammonium formate (55:45) containing 1 g of ascorbic acid/L of eluent; flow rate: 5 mL/min). The product, eluted off at ~13.5 min, was isolated from the HPLC solvent by solid-phase extraction with a C18 Sep-Pak, and then formulated with ethanol (1 mL) and 0.1% ascorbic acid in sterile saline (10 mL), with a final ethanol concentration of < 10% (vol/vol). The product solution was sterilized prior to dispensing by passage through a 0.22-μm membrane filter. Purity and specific activity of the final product was determined by analytical HPLC (Luna C18(2) column, 5 μm, 4.6 × 250 mm; mobile phase: acetonitrile/0.1 M ammonium formate (55:45); flow rate: 2 mL/min). Identity of the tracer was confirmed by co-injection with a sample of the standard. The chemical and radiochemical purities were >95%, with specific activity of 4.7 ± 1.5 mCi/nmol at end of synthesis.

TABLE I. Scan parameters

	Plasma free fraction	Injected dose (mCi/kg)	Injected mass (μg/kg)	Specific activity (mCi/nmol)
Baseline test	3.0 ± 0.1%[a]	0.17 ± 0.03	0.022 ± 0.001	2.0 ± 0.3
Retest	3.1 ± 0.1%[a]	0.14 ± 0.08	0.021 ± 0.005	1.6 ± 0.7
Baseline NAC 1	3.3 ± 1.0%	0.34 ± 0.34	0.066 ± 0.074	1.9 ± 0.8
Post NAC 1	2.9 ± 0.1%	0.32 ± 0.35	0.045 ± 0.040	2.3 ± 1.6
Baseline NAC 2	3.4 ± 0.8%	0.23 ± 0.08	0.029 ± 0.007	2.0 ± 0.1
Post NAC 2	3.2 ± 0.2%	0.13 ± 0.06	0.022 ± 0.001	1.4 ± 0.6

[a]Plasma free fraction in test-retest group only available for two monkeys. Specific activity was at time-of-injection. There was no significant difference between groups ($P < 0.05$).

Input function measurements

The input functions, corresponding to the arterial plasma concentration corrected for the presence of radiometabolites, were generated for all but one scan. Samples (~0.5 mL) of arterial blood were manually drawn throughout the study. Plasma was separated from blood cells via centrifugation (3900*g* for 5 min at 4°C), and radioactivity was counted in a cross-calibrated well counter (Wizard 1480, Perkin Elmer, Waltham, MA).

Plasma analysis of the radiotracer metabolism was performed from arterial blood samples collected at 4, 10, 30, 60, and 90 min after injection using the column switching HPLC method (Hilton et al., 2000) to determine the parent fraction. Plasma samples were treated with urea (8 M) and loaded onto a capture column (19 × 4.6 mm) packed with Phenomenex SPE C18 Strata-X sorbent and eluted with 1% acetonitrile in water at a flow rate of 2 mL/min. At 4 min, the activity trapped on the capture column was back-flushed onto an analytical HPLC column (Phenomenex Synergy Polar-RP, 5 μm, 250 × 4.6 mm) eluting with 45% acetonitrile in 0.1 M ammonium formate at a flow rate of 1.65 mL/min. The HPLC eluent was collected with a Spectrum Chromatography CF-1

automated fraction collector. The unmetabolized parent fraction, with retention time of ~7 min after column switching, was determined as the ratio of the sum of radioactivity in fractions containing the parent to the total amount of radioactivity collected and was fitted with two functions, a bounded sum of exponentials or an inverted gamma function; the model that provided the best fit was used, independent of study group. This fraction curve was also corrected by the time-varying extraction efficiency of radioactivity in the corresponding filtered plasma sample. The final plasma input function was calculated as the product of the total plasma curve and the parent fraction curve.

An ultrafiltration-based method was used for measuring the unbound portion (free fraction, f_p) of [^{11}C]ABP668 in plasma, with 150 μCi of [^{11}C]ABP668 added to 3.0 mL of arterial blood sample taken immediately before tracer injection. After 10 min incubation at room temperature, the spiked blood sample was centrifuged at 2930*g* for 5 min. Plasma (0.3 mL) was separated and loaded onto the reservoir of the Millipore Centrifree® micropartition device in triplicates and centrifuged at 1228*g* for 20 min. The free fraction was determined by calculating the ratio of the radioactivity concentration in the ultrafiltrate to the total activity in plasma.

MRI scanning and processing

Magnetic resonance (MR) images were acquired on a Siemens Magnetom 3.0 T Trio scanner, using an extremity coil. T_1-weighted images were acquired in coronal plane with spin echo sequence (TE (echo time) = 3.34, TR (repetition time) = 2530, flip angle = 7°, section thickness = 0.50 mm, field-of-view = 140 mm, image matrix = 256 × 256 × 176 pixels, matrix size = 0.55 mm × 55 mm × 0.50 mm). The MR images were stripped of skull and muscle so that only the brain remained in the image (FMRIB's Brain Extraction Tool, http://www.fmrib.ox.ac.uk/fsl/bet2/index.html). This skull and muscle stripping procedure was performed once for each monkey's MR image prior to co-registration with the PET images.

PET image reconstruction and processing

Listmode data were collected and reconstructed using filtered backprojection (FBP) with all corrections (attenuation, normalization, scatter, randoms, and deadtime) into a sequence of 27 frames: 6 × 30 sec; 3 × 1 min; 2 × 2 min; 16 × 5 min. Final image dimensions and voxel sizes were 256 × 256 × 95 and 0.95 × 0.95 × 0.80 mm^3, respectively.

PET images were aligned to the MR via a 6-parameter rigid registration with the Multi-Transform Method (Sandiego et al., 2013) to generate the optimal transformation to map the PET dynamic data into the monkey's MR image space. An affine linear + nonlinear registration was performed (Bioimage Suite 2.5, http://www.bioimagesuite.org/index.html) for each MR image to a high-resolution rhesus monkey MR template where regions-of-interest (ROIs) were defined. The ROIs were then mapped from the template to PET space via the two transforms (e.g., PET-MR and MR-template) to compute time–activity curves (TACs) in the following regions: CGM (1.27 cm^3), cingulate (0.64 cm^3), occipital (5.2 cm^3), frontal (2.5 cm^3), temporal (3.2 cm^3), caudate (0.43 cm^3), and putamen (0.34 cm^3).

Tracer kinetic modeling

The outcome measures for this study were the total volume of distribution (V_T) and the non-displaceable binding potential (BP_{ND}) for [^{11}C]ABP688 (Innis et al., 2007). V_T (mL cm^{-3}) is the equilibrium tissue to plasma activity ratio, and BP_{ND} (unitless) is the ratio of specific to free plus non-specific bound radioligand binding at equilibrium, where a non-displaceable reference region is used to represent the free and non-specifically bound tracer. Four modeling methods were used for the kinetic analysis of regional [^{11}C]ABP688 TACs: 1-Tissue (1T) and 2-Tissue (2T) compartment models, multi-linear analysis (MA1), and simplified reference tissue model (SRTM). The arterial input function was used to estimate parameters for 1T, 2T, and MA1 ($t^* = 40$ min) models to compute V_T (Gunn et al., 2001; Ichise et al., 2002). For these models, BP_{ND} was computed as

$$BP_{ND} = \frac{V_T(\mathrm{ROI})}{V_T(\mathrm{CGM})} - 1, \quad (1)$$

where V_T(ROI) and V_T(CGM) are the volumes of distribution in the ROI and the CGM reference region, respectively.

SRTM requires a reference region to estimate BP_{ND} without the need for an arterial input function (Lammertsma and Hume, 1996). With the CGM as reference input, BP_{ND} was computed as

$$BP_{ND} = R_1 \frac{k_2'}{k_2} - 1, \quad (2)$$

where R_1, k_2, and k_2' parameters are estimated directly from SRTM. $R_1 = K_1/K_1'$ where K_1 and K_1' (mL cm^{-3} min^{-1}) are the rate constants of tracer influx from the blood to tissue in the ROI and reference tissue, respectively. Parameters k_2 (min^{-1}) and k_2' (min^{-1}) are the rate constants of tracer efflux to the blood from the tissue in the ROI and reference tissue, respectively.

Data were weighted in the fits using an approximation of noise-equivalent counts for each frame (Pajevic et al., 1998). The models were evaluated in terms of quality of fit to the data and percent

standard error (%SE), where %SE = SE/(V_T or BP_{ND}) × 100 for V_T and BP_{ND}, and SE is the estimated parameter standard error calculated from the inverse of the Fisher information matrix (Delforge et al., 1990). Fit quality was evaluated between 1T and 2T models using the F test ($P < 0.05$). Reliability of V_T and BP_{ND} estimates from each model were compared for fits with %SE less than 20% across all models, with the 2T model as the standard for comparison.

Percent change in V_T (%ΔV_T) and BP_{ND} (%ΔBP_{ND}) from baseline to post-NAC were computed as

$$\%\Delta V_T = \left(\frac{V_T(\text{NAC})}{V_T(\text{Baseline})} - 1\right) \times 100 \quad (3)$$

and

$$\%\Delta BP_{ND} = \left(\frac{BP_{ND}(\text{NAC})}{BP_{ND}(\text{Baseline})} - 1\right) \times 100. \quad (4)$$

Equation (4) was also used to compute %ΔBP_{ND} for test-retest studies, with BP_{ND} (Retest) in the numerator and BP_{ND} (Test) in the denominator. Data are reported as mean ± s.d. Statistical analysis within each group was performed with two-tailed, paired t-tests with $P < 0.05$, without correction for multiple comparisons.

RESULTS

Scan parameters

Scan parameters are shown in Table I. Within and between groups, there were no significant differences in plasma free fraction, injected dose, injected mass, or specific activity. Plasma free fraction measurements were only available for two monkeys in the test-retest group. Mean injected dose was slightly higher for the baseline-NAC 1 group due to higher activity injected for the bolus plus infusion study. In addition, injected mass was higher in the baseline-NAC 1 group for one study where the mass limit was originally set to 0.25 μg/kg, but was lowered to 0.025 μg/kg for subsequent studies to match the mass limit in the baboon study (Miyake et al., 2011).

Regional brain distribution of [^{11}C]ABP688

Figure 2 shows averaged [^{11}C]ABP688 images normalized via linear and nonlinear registrations to a high-resolution rhesus monkey brain template in sagittal, coronal, and axial views. The early summed image (0–10 min postinjection, $n = 8$) shows a uniform distribution of [^{11}C]ABP688 throughout the gray matter (Fig. 2B). The later image (40–60 min) shows a heterogeneous distribution of tracer in the brain, with lower uptake in the CGM reference region (Fig. 2C).

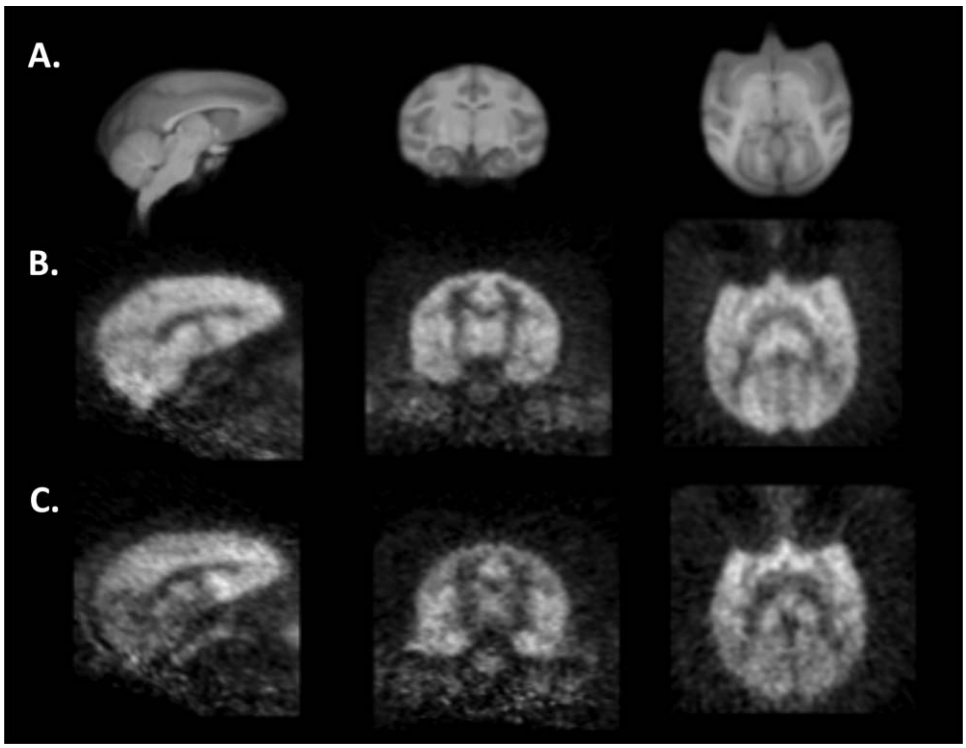

Fig. 2. An average of eight 0–10 min and 40–60 min summed [^{11}C]ABP688 images under baseline condition normalized to a nonlinear rhesus monkey brain MR template in sagittal, coronal, and transverse views (left to right). **A**: The high-resolution rhesus monkey brain template was used to delineate ROIs. **B**: Early 0–10 min summed images exhibited uniform distribution throughout the gray matter. **C**: Late 40–60 min summed images show a less homogenous distribution with lower uptake in the CGM, which was used as the reference region.

Model comparison

Model fits

TACs and typical model fits for 1T, 2T, MA1, and SRTM are shown in Figure 3. The 1T model produced visually poorer quality fits to the data, whereas the 2T model fit the data better for 83% of ROI curve fits, as determined by the F test [$F(2,23) = 3.42$, $P < 0.05$] (Figs. 3A and 3B). For MA1, t^* was chosen to be 40 min, which provided reasonable fits to the data (Fig. 3C) and good agreement with 2T estimates of V_T and BP_{ND} (see below). Fits were generally good for MA1 with $t^* = 30$ min but were of poorer quality with $t^* = 20$ min. SRTM also provided visually good fits to the data (Fig. 3D). Generally, the 2T model would be considered the standard, since the quality of fits was superior to 1T, based on the F-test. However, many unreliable estimates were produced with percent standard errors (%SE) exceeding 20% for V_T (6% of fits) and BP_{ND} (45% of fits). Therefore, a surrogate model was needed to analyze the data.

Model comparison

V_T values were compared in all ROIs where %SE was less than 20% for 1T and MA1 vs. 2T (Supporting Information Fig. 1). The 1T model underestimated V_T compared with 2T, where $V_T(1T) = 0.81V_T(2T) + 0.76$, $R^2 = 0.95$ (Supporting Information Fig. 1A). V_T estimates from MA1 with $t^* = 40$ min agreed very well with those of 2T, where $V_T(MA1) = 1.00V_T(2T) + 0.30$, $R^2 = 0.98$ (Supporting Information Fig. 1B) compared with V_T estimates from MA1 with t^* at 30 or 20 min: $V_T(MA1, t^* = 30) = 0.96V_T(2T) + 0.50$, $R^2 = 0.98$, and $V_T(MA1, t^* = 20) = 0.92V_T(2T) + 0.68$, $R^2 = 0.98$.

BP_{ND} values were compared in all ROIs where %SE was less than 20% for 1T, MA1, and SRTM vs. 2T (Supporting Information Fig. 2). 1T and MA1 estimates of BP_{ND} were slightly biased compared to 2T values with $BP_{ND}(1T) = 1.07BP_{ND}(2T) + 0.05$, $R^2 = 0.95$ (Supporting Information Fig. 2A) and $BP_{ND}(MA1) = 0.92BP_{ND}(2T) + 0.00$, $R^2 = 0.93$ (Supporting Information Fig. 2B). SRTM estimates of BP_{ND} were negatively biased compared with 2T, where $BP_{ND}(SRTM) = 0.88BP_{ND}(2T) + 0.02$, $R^2 = 0.97$ (Supporting Information Fig. 2B).

Thus, all models had moderate biases compared with 2T; however, in all cases there was high correlation for V_T and BP_{ND} estimates. 1T had the most

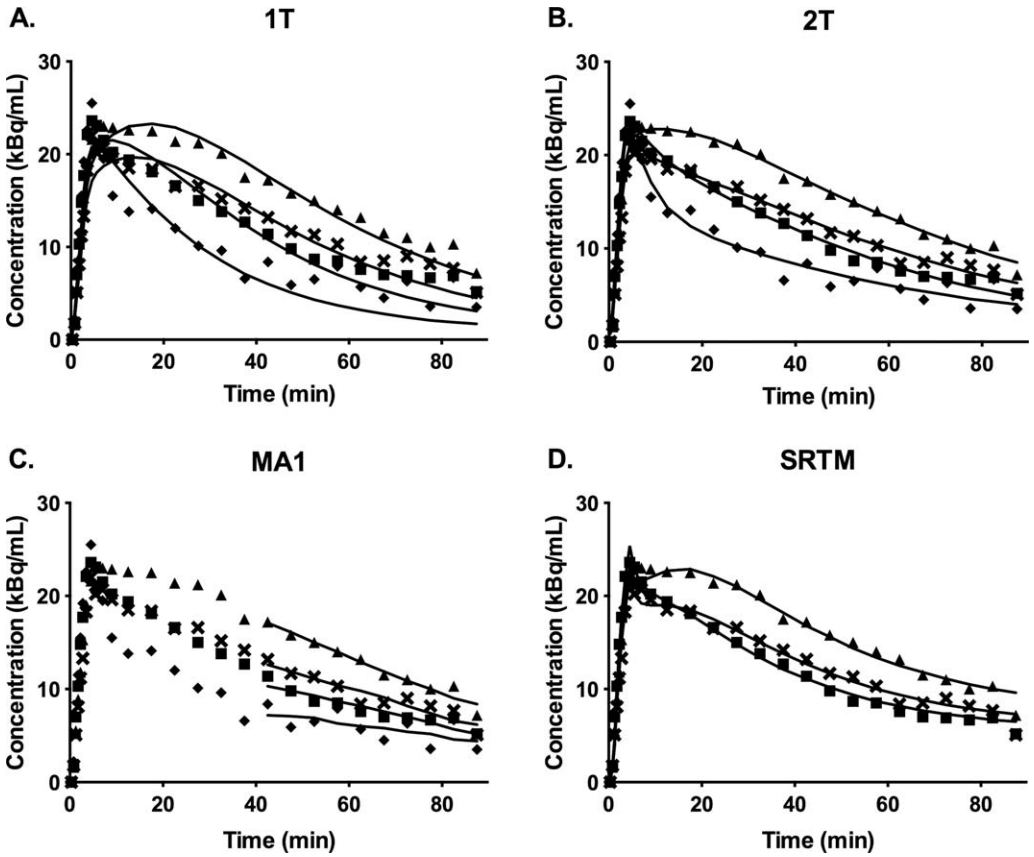

Fig. 3. Time–activity curves for the frontal (▲), temporal (×), occipital (■), and CGM (◆) regions and typical model fits for (**A**) 1T, (**B**) 2T, (**C**) MA1, and (**D**) SRTM. The 1T model produced visually poorer quality fits to the data, whereas the 2T model fitted the data better for 83% of ROI curve fits [$F(2,23) = 3.42$, $P < 0.05$]. MA1 and SRTM provided reasonable fits to the data.

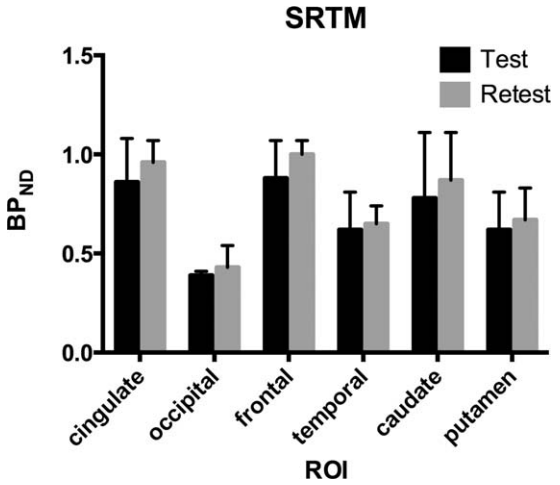

Fig. 4. Test-retest [^{11}C]ABP688 BP_{ND} derived with SRTM ($n = 3$). BP_{ND} increased from the test to retest scan, although the change was not significant. Error bars are standard deviations. SRTM was used for analysis due to lack of arterial input function data for one animal.

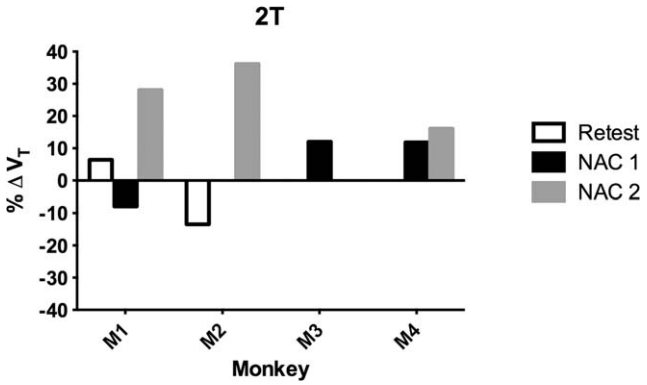

Fig. 5. Percent change in V_T ($\%\Delta V_T$) with 2T analysis of the CGM from test/baseline to retest ($n = 2$), NAC 1 (50 mg/kg, $n = 3$), and NAC 2 (100 mg/kg, $n = 3$) for each monkey. Monkey 1 (M1) was scanned in all three groups. Monkey 2 (M2) was in the retest and the NAC 2 group, and Monkey 3 (M3) was in the NAC 1 group. Monkey 4 (M4) was in both NAC 1 and NAC 2 groups. Mean $\%\Delta V_T$ with NAC 2 increased significantly ($P < 0.05$).

stable estimates of V_T ($\%SE(V_T) > 20\%$: 1T(0%), 2T(6%), and MA1(2%)), however the 1T fit quality was poorer than the other models. Fit quality for MA1 and SRTM was good. MA1 had the closest agreement for estimation of V_T with 2T. For BP_{ND}, SRTM had the most stable estimates of BP_{ND} ($\%SE(V_T) > 20\%$: 1T(16%), 2T(46%), MA1(22%), and SRTM(5%)). Overall, there was no clear best model surrogate for the 2T model, therefore MA 1 and SRTM methods were used to analyze the NAC data.

Test-retest study

Test-retest BP_{ND} was analyzed with SRTM ($n = 3$) due to the lack of arterial input data for one of the three monkeys. BP_{ND} increased from test to retest in all regions: cingulate ($15 \pm 16\%$), occipital ($10 \pm 29\%$), frontal ($17 \pm 27\%$), temporal ($9 \pm 24\%$), caudate ($17 \pm 19\%$), and putamen ($10 \pm 8\%$) (Fig. 4). Test-retest V_T ($n = 2$) also increased for ROIs with MA1 ($9 \pm 4\%$) (data not shown). Globally, BP_{ND} was lower by $13 \pm 19\%$ in test scans compared with retest scans.

Cerebellum gray matter V_T

The percent change in V_T ($\%\Delta V_T$) in the CGM reference region from test/baseline for retest ($n = 2$), NAC 1 ($n = 3$), and NAC 2 ($n = 3$) for each monkey is shown for the 2T model in Figure 5. Mean $\%\Delta V_T$ across animals is shown with the MA 1 model for both NAC groups in Figure 6. With 2T, the fit quality was good and %SE in V_T estimates was less than 20%. The following analysis is reported for the CGM with 2T and is consistent with MA1. There were no differences in $\%\Delta V_T$ between test-retest ($n = 2$) and post-NAC ($n = 6$) scans, respectively ($-4 \pm 14\%$ and $16 \pm 15\%$, $P = 0.12$) (two-tailed, unpaired t-test, $P < 0.05$). The unpaired t-test was used because different combinations of animals were used for each group with some overlap (Fig. 5). Only two of the three animals in the test-retest group had an arterial input function, and three animals per NAC 1 and NAC 2 groups had paired baseline-NAC scans. Pooling NAC 1 and NAC 2 groups ($n = 6$) compared with paired baseline data ($n = 6$), $\%\Delta V_T$ in the CGM increased significantly ($12 \pm 13\%$, $P = 0.04$). The NAC 2 group mainly drove the increase in CGM V_T significantly from baseline ($29 \pm 7\%$, $P = 0.02$). Thus, the NAC 1 dose (50 mg/kg) produced no change, but the NAC 2 dose (100 mg/kg) significantly increased CGM V_T from baseline. There was no difference in CGM $\%\Delta V_T$ between NAC 1 and NAC 2 challenge groups. Moreover, $\%\Delta V_T$ in the CGM was not different between combined baseline-NAC and test-retest groups.

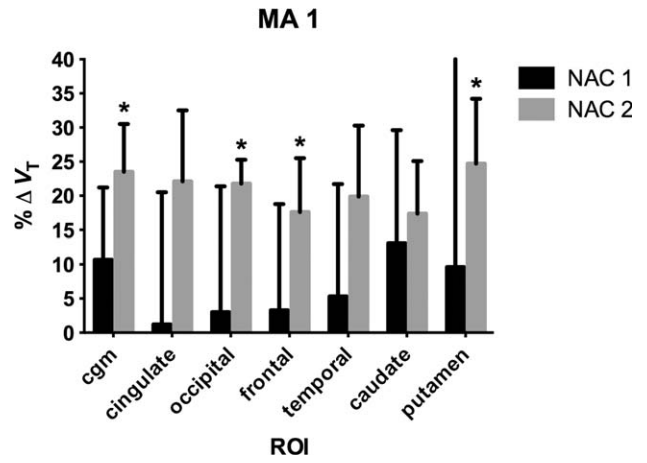

Fig. 6. Regional percent change in V_T ($\%\Delta V_T$) from baseline after NAC 1 (50 m/kg) and NAC 2 (100 mg/kg) from MA1 ($^*P < 0.05$). Error bars are standard deviations.

TABLE II. Baseline and post-NAC V_T and %Δ V_T with MA1

	Baseline 1	NAC 1	%Δ V_T	*P*	Baseline 2	NAC 2	%Δ V_T	*P*
CGM	8.4 ± 3.5	9.5 ± 4.6	10.7 ± 10.5	0.26	5.9 ± 2.2	7.2 ± 2.4	23.5 ± 7.0	0.02
Cingulate	14.9 ± 4.2	15.6 ± 6.8	1.2 ± 19.3	0.69	11.3 ± 3.1	13.7 ± 3.7	22.1 ± 10.4	0.06
Occipital	10.7 ± 3.4	11.4 ± 5.1	3.0 ± 18.4	0.57	8.2 ± 2.3	10.0 ± 2.8	21.8 ± 3.5	0.03
Frontal	14.2 ± 3.2	15.0 ± 5.4	3.3 ± 15.5	0.60	11.6 ± 2.8	13.5 ± 2.8	17.6 ± 7.9	0.04
Temporal	12.7 ± 4.0	13.8 ± 6.0	5.3 ± 16.4	0.43	9.8 ± 3.0	11.6 ± 3.1	19.9 ± 10.4	0.06
Caudate	13.3 ± 3.9	15.4 ± 6.4	13.1 ± 16.5	0.27	10.0 ± 2.5	11.8 ± 3.5	17.4 ± 7.7	0.10
Putamen	11.9 ± 2.9	13.6 ± 6.6	9.6 ± 30.7	0.51	8.8 ± 2.7	10.9 ± 2.7	24.7 ± 9.5	0.02

Significance level was $P < 0.05$ (two-tailed, paired *t*-test) of the difference between the baseline and post-NAC scans.

NAC challenge

Regional $\%\Delta V_T$ post-NAC is shown for the MA1 model in Figure 6 with mean V_T pre- and post-NAC shown in Table II, including the cerebellum. From the NAC 1 group, the 2nd highest change in V_T was 11% in the cerebellum, where the changes were less than 5% in the larger cortical regions. From the NAC 2 group, the 2nd highest change in V_T was 24% in the cerebellum and was more comparable to the changes observed in the other regions, suggesting a global effect of NAC. There was no change in V_T from baseline after the 50 mg/kg NAC challenge (NAC 1 group). However, there was a significant increase in $\%\Delta V_T$ from baseline after the 100 mg/kg NAC challenge (NAC 2 group) in multiple regions: CGM ($24 \pm 7\%$, $P = 0.02$), occipital ($22 \pm 4\%$, $P = 0.03$), frontal ($18 \pm 8\%$, $P = 0.04$), and putamen ($25 \pm 10\%$, $P = 0.02$).

Percent change in BP_{ND} post-NAC is shown in Figure 7 with MA1 and SRTM methods for cortical regions (cingulate, occipital, frontal, and temporal). Generally, both models show a reduction in BP_{ND} from baseline after both NAC 1 and NAC 2 challenges. Mean cortical $\%\Delta BP_{ND}$ from baseline-post NAC 1 and baseline-post NAC 2, respectively, were not significant with MA1 ($-16 \pm 21\%$ and $-5 \pm 11\%$, $P = 0.19$) and SRTM ($-3 \pm 12\%$ and $-10 \pm 7\%$, $P = 0.08$). Variability was lowest with SRTM, revealing a possible dose-dependent decrease in BP_{ND} from NAC 1 to NAC 2 groups compared with the respective baselines.

The overall effect of NAC on $\%\Delta V_T$ and $\%\Delta BP_{ND}$ with MA1 was compared for cortical regions after pooling together all of the baseline ($n = 6$) and NAC challenge ($n = 6$) data shown in Figure 8. The mean global effect was a $13 \pm 14\%$ increase in V_T and a $10 \pm 17\%$ reduction in BP_{ND} from baseline. There was a significant difference between NAC and baseline V_T only in the CGM and the caudate regions, but no regional differences in BP_{ND} between NAC and baseline. In addition, there was no difference between test-retest $\%\Delta BP_{ND}$ ($n = 3$) and baseline-NAC $\%\Delta BP_{ND}$ ($n = 6$) (2-tailed, unpaired *t*-test, $P < 0.05$).

Comparison of BP_{ND} for test-retest and baseline-NAC studies: Monkey vs. baboon

Test-retest and baseline-NAC $\%\Delta BP_{ND}$ from the current study in rhesus monkeys was compared directly with the Miyake et al. study in baboons (Fig. 9). BP_{ND} was computed from SRTM for monkeys (Eq. (2)) and with 2T for baboons (Eq. (1)). There was no change in BP_{ND} (~5%) in baboons ($n = 3$) from

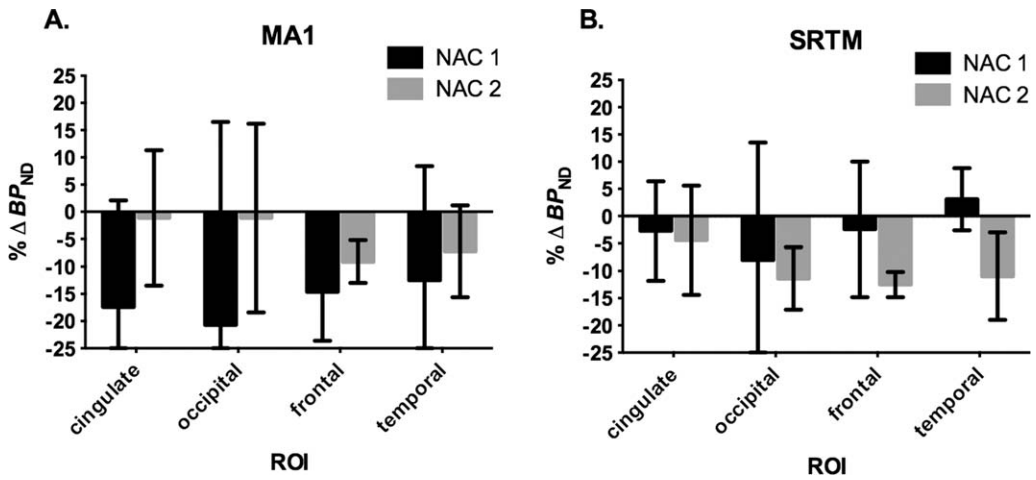

Fig. 7. Percent change in BP_{ND} ($\%\Delta BP_{ND}$) from baseline after NAC in cortical regions. Models (**A**) MA1 and (**B**) SRTM show reductions in $\%\Delta BP_{ND}$ for cortical regions after both NAC 1 and NAC 2 doses, except in the temporal region with SRTM. Error bars are standard deviations.

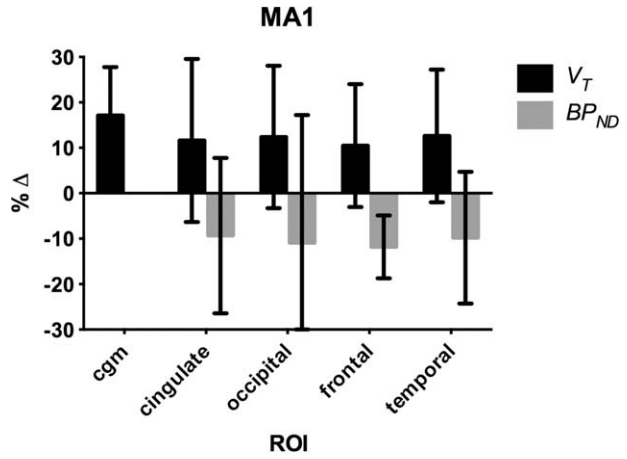

Fig. 8. Percent change (%Δ) in V_T and BP_{ND} from baseline with all NAC studies ($n = 6$) with MA1. Error bars are standard deviations.

test to retest but a non-significant increase (~10–20%) from test to retest scans in monkeys ($n = 3$) (Fig. 9A). BP_{ND} decreased in the monkeys (3–13%) after the 50 mg/kg ($n = 3$) and 100 mg/kg ($n = 3$) NAC doses, however, reduction in BP_{ND} at the 50 mg/kg dose in the baboons ($n = 3$) was larger (13–21%) (Fig. 9B). Variability was similar between monkeys and baboons, respectively, for test-retest (16–29% vs. 14–20%) and NAC studies (6–21% vs. 5–13%) (Fig. 9).

DISCUSSION

The goal of this study was to replicate and extend the baboon study of Miyake et al. (2011) regarding the assessment of NAC-induced glutamate changes with the mGluR5 tracer [^{11}C]ABP688. This study did not replicate the results of Miyake et al. (2011), but components of our rhesus monkey data are consistent with the baboon results based on BP_{ND}. High inter-subject variability was common between the baboon and monkey studies. The net effect of NAC on [^{11}C]ABP688 BP_{ND} in this study may have been similar to Miyake et al. (2011), if the global increase in test-retest BP_{ND} (Fig. 4) is included. For instance, combining the $\%\Delta BP_{ND}$ from test-retest to the $\%\Delta BP_{ND}$ from baseline-NAC (50 mg/kg) and baseline-NAC (100 mg/kg), respectively, would have produced a net reduction in BP_{ND} (i.e., cingulate (18% and 19%), occipital (18% and 21%), frontal (19% and 30%), and temporal (6% and 20%)) similar to the baboon study at baseline-NAC (50 mg/kg) (i.e., cingulate (21%), occipital (25%), frontal (21%), and temporal (18%)) (Fig. 9).

Mechanism of NAC

NAC is currently used as an antioxidant, a mucolytic agent, as well as for paracetamol overdose, with many potential therapeutic uses toward psychiatric illnesses (Dean et al., 2011; Dodd et al., 2008). NAC, a pro-drug for cysteine, indirectly facilitates non-vesicular glutamate transmitter release into the non-synaptic extracellular space via the cysteine-glutamate antiporter, where extracellular cysteine is exchanged for intra-cellular glutamate (Baker et al., 2002). Although little is understood about the direct interaction between modulating glutamate transmission and mGluR5 receptor function, a study showed that NAC ameliorated prepulse inhibition deficits (PPI) (relevant in schizophrenia) in mGluR5 knock-out mice, providing further evidence for close interactions between mGluR5 and NMDA receptors involved in PPI regulation (Chen et al., 2010). Another study showed that NAC pretreatment in phencyclidine rat models of schizophrenia alleviated withdrawal symptoms and restored working memory, where restoration in working memory due to NAC was reversed with a cysteine-glutamate antiporter inhibitor (Baker et al., 2008). Our findings together with the

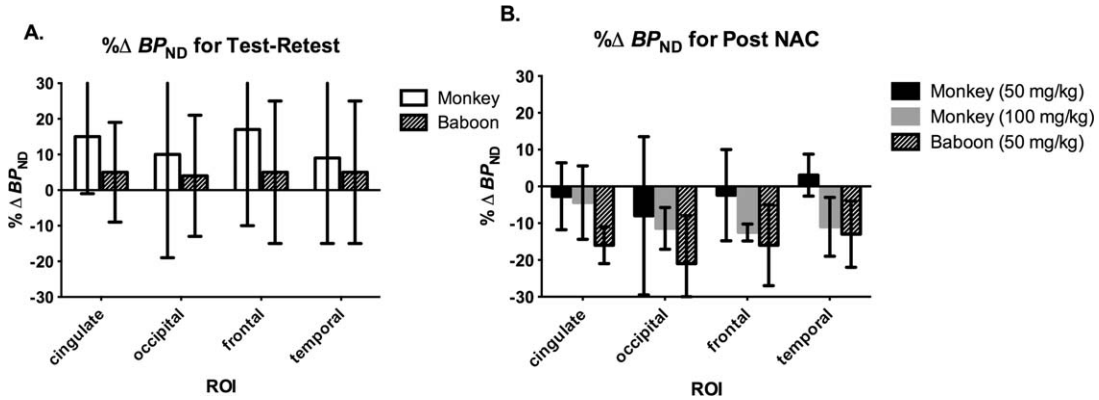

Fig. 9. Comparison of BP_{ND} changes in the current study to those of the Miyake et al., (2011) study in baboons. (**A**): Percent change in BP_{ND} ($\%\Delta BP_{ND}$) for test-retest in monkeys ($n = 3$) and baboons ($n = 3$) and (**B**) %Δ BP_{ND} after NAC challenge for monkeys (50 mg/kg, $n = 3$ or 100 mg/kg, $n = 3$) and baboons (50 mg/kg, $n = 3$). BP_{ND} was computed from SRTM for monkeys (Eq. (2)) and with 2 T for baboons (Eq. (1)). Error bars are standard deviations.

preliminary PET findings (Miyake et al.), suggest that NAC-induced increases in endogenous glutamate may be indirectly measureable at the mGluR5 allosteric site with [^{11}C]ABP688. However, a more reliable radiotracer with better test-retest reproducibility is necessary to fully assess this effect.

Modeling methods

Since there was no obvious best choice of modeling method, different methods were used to analyze and interpret the data. Although the 2T model fit the data well visually and statistically, based on the *F*-test in comparison to the 1T model, V_T and BP_{ND} estimates were unstable (i.e., %SE>20%), and a surrogate model was needed. The 1T model was dropped from the analysis based on poorer quality fits as compared with the MA1 and SRTM models. Compared with 2T, MA1 and SRTM had moderate biases and estimates of V_T and BP_{ND} were highly correlated to the 2T values (Supporting Information Figs. 1 and 2). MA1 provided good agreement to the 2T values (with lower %SE), so only MA1 and SRTM results were presented, with the cerebellum as an exception where 2T results were shown (Fig. 5). Subcortical ROIs, i.e., caudate and putamen, were excluded from analysis with BP_{ND} due to large %SE in estimates. Factors contributing to high %SE, particularly for small subcortical ROIs, include noise in high-resolution Focus-220 data and low injected activity due to low mass dose. In addition, images were reconstructed with FBP, which is less biased but noisier compared with OSEM (ordered subsets-expectation maximization)-reconstructed images.

Intersubject and intrasubject variability

A challenging aspect of this study is the substantial variability, which limits the power to detect changes in a small study. Large intersubject variability has been consistent among outcome measures of [^{11}C]ABP688 in human and nonhuman primate studies. Direct comparison of the current study in monkeys and the Miyake et al. study in baboons in Figure 9 showed similar variability in $\%\Delta BP_{ND}$ for both species ranging from 6 to 29% and 5 to 20%, respectively, for test-retest and baseline-NAC challenge studies. For instance, baseline [^{11}C]ABP688 BP_{ND} across regions ranged from 0.18 to 0.61 in one monkey from 0.37 to 0.92 in another monkey. In the human study with [^{11}C]ABP688, variability in percent difference from test to retest was as high as 17% for V_T and 40% for BP_{ND} between subjects ($n = 8$) (DeLorenzo et al., 2011a).

Three animals had more than one baseline scan with the same timing post-ketamine (~2 h) from different days. This permitted an evaluation of intrasubject variability. One monkey had three baseline scans and two monkeys had two baseline scans, and the percent coefficient of variation (%COV = s.d./mean × 100) across scans was computed. Repeated baseline values across animals and regions had a COV of $8 \pm 4\%$ for V_T. For the three monkeys, V_T in the cerebellum at baseline was 4.46 ± 0.53, 5.84 ± 0.59, and 8.70 ± 0.62. However, intrasubject variability in BP_{ND} was greater, averaging $20 \pm 13\%$ across animals and regions. This variability in BP_{ND} contributes to the challenges to detect meaningful biological signals, especially in small samples.

Test-retest increases in BP_{ND} and V_T increases after NAC

We found a trend toward increasing [^{11}C]ABP688 BP_{ND} from test to retest that was not evident in Miyake et al. (Fig. 4). In that study, baboons were induced with ketamine prior to the first scan in a paired-bolus design. However, the exact timing between ketamine induction and tracer injections was unclear. Interestingly, test-retest studies with [^{11}C]ABP688 in humans showed a significant and consistent increase in V_T and BP_{ND} across regions, and the increases were attributed to physiological changes which altered glutamate from morning to afternoon scans (DeLorenzo et al., 2011a). Because the current study is in anesthetized nonhuman primates, we assume no specific physiological changes are occurring over the course of the day. One potential explanation for test-retest increases in monkeys may be due to effects at mGluR5 from anesthetic induction with ketamine (10 mg/kg, IM), administered 2 h prior to the first [^{11}C]ABP688 injection that were not present in the second scan (~5 h after ketamine) (see Fig. 1 for study design). As mentioned previously, it is well established that mGluR5 and NMDA receptors are co-localized post-synaptically and function synergistically in response to glutamate transmission (Chen et al., 2010; Perroy et al., 2008). While subanesthetic doses of ketamine, a non-competitive NMDA receptor antagonist, have been shown to increase glutamate levels in the rat brain, anesthetic doses of ketamine decreased or did not change glutamate levels (Chowdhury et al., 2012; Moghaddam et al., 1997). Thus, based on that finding, we do not expect that the anesthetic dose of ketamine used in the current study (2 h prior to the initial radiotracer injection) influenced test-retest reliability. However, given that any residual ketamine levels would be much smaller by the time of the first [^{11}C]ABP688 administration, it is possible that this lower level of ketamine produced a glutamate-related effect.

To examine whether ketamine had an effect on test-retest results, data were analyzed with MA1 for two animals, where repeated baseline scans (2 h post-ketamine) on different days were compared with their retest scans (5 h post-ketamine). One monkey (M1) had three baseline scans and one retest scan,

and the other monkey (M2) had two baseline scans and one retest scan. Percent increase in V_T from the mean of the baseline scans and the retest scans were computed across regions for each monkey. However, the results were not consistent; the mean percent increases in V_T from average baseline to retest across all regions were $+15 \pm 4\%$ and $0 \pm 1\%$ for M1 and M2, respectively. For the cerebellum, these changes were +34% and −8% for M1 and M2, respectively. Based on this analysis, it is still unclear whether ketamine is lowering "baseline" V_T as compared with re-test scans. In order to fully evaluate the potential effects of ketamine, additional studies in a larger cohort are required.

Another possible reason for increases in V_T may be increases in tracer plasma free fraction (f_p) from the first to the second scan. However, changes in f_p were small and were not different from the 1st to the 2nd scan. Measurement of f_p was performed with an ultrafiltration-based method, and reliability of measurements is of concern as [^{11}C]ABP688 has high protein binding and appears to adhere to the filter. Another method for measuring f_p, equilibrium dialysis, may provide more reliable measurements for free fraction (Gunn et al., 2012), but was not used for this study.

Dose-dependent decrease in BP_{ND} from NAC1 to NAC 2

A dose-dependent decrease in [^{11}C]ABP688 BP_{ND} from baseline to NAC 1 (50 mg/kg) and baseline to NAC 2 (100 mg/kg) was observed with SRTM (Fig. 7B). This trend was not observed with MA1 (Fig. 7A), possibly due to the higher %SE in outcome measure estimates compared with SRTM. The validity of a dose-dependent change would be best supported with plasma analysis for NAC. Another approach to assess occupancy is with the occupancy plot, which may be implemented without a true reference region or baseline data (Cunningham et al., 2010). However, the occupancy plot was not found to be useful for this dataset due to large variability and the increases in V_T after the NAC 2 challenge.

Cerebellum as a reference region

An appropriate reference region is important to provide quantitative estimates of BP_{ND}. A suitable reference region is also helpful to eliminate the need for arterial blood samples. A metabolite-corrected input function is required for 1T, 2T, and MA1 models. Instead, reference region modeling (i.e., SRTM) or bolus plus constant infusion approaches can be used to determine BP_{ND}. A reference ROI is validated via blocking studies, where lack of reduction in V_T, compared with baseline, indicates a region devoid of specific receptor binding for the radioligand of interest.

Reference tissue model approaches were validated in rats with [^{11}C]ABP688 test-block studies with 1,2-methyl-6-(phenylethynyl)-pyridine MPEP (mGluR5 NAM) with in vivo PET and in vitro autoradiography and saturation binding studies (Elmenhorst et al., 2010). The cerebellum was proven as a viable reference region based on negligible change in [^{11}C]ABP688 V_T after blockade with MPEP, good correlation between arterial input and reference input modeling approaches to estimate BP_{ND}, significant correlation between BP_{ND} and B_{max} measurements, and agreement of non-displaceable V_T (V_{ND}) between the Lassen graphical approach and 2T estimation of cerebellum V_T. In baboons, a [^{11}C]ABP688 test-block study with MTEP (mGluR5 NAM) showed the smallest change (~7%) in the CGM V_T, and this provided further support for the cerebellum as a reference region (DeLorenzo et al., 2011b). SRTM produced a similar bias of BP_{ND} estimates compared with 2T between this and the previous study (DeLorenzo et al., 2011b), where SRTM underestimated 2T BP_{ND} by 16% and 12%, respectively.

The preliminary study in baboons showed no change in cerebellum [^{11}C]ABP688 V_T after NAC (50 mg/kg) (Miyake et al., 2011) consistent with our study at the same dose. However, we found a significant increase in CGM V_T (20–30%) after the 100 mg/kg NAC challenge across 2T and MA1 models. Activity in the cerebellum, corrected for injected dose, was consistently higher in the NAC scans compared with the baseline scans by a mean of 29% from 40 to 90 min postinjection. There was no consistent change in the metabolite-corrected plasma concentration during that time. Thus, increases in cerebellum V_T after NAC are likely driven primarily by the higher cerebellum tissue concentration.

The $\%\Delta V_T$ post-NAC observed in the cerebellum was similar, or sometimes larger than the percent changes observed in other regions (Fig. 6). Given that the fraction of specific binding in the cerebellum is smaller than that of other regions (Fig. 3), it may be that there is a mechanism producing increases in V_T that is unrelated to a change in specific binding. Rather, the data suggest that there could be a global effect of NAC, increasing V_T in all regions (such as an increase in f_P), plus a second effect on specific binding that is region-dependent. This combination of effects could explain increases in V_T and decreases in BP_{ND}.

The increase in CGM V_T post-NAC 2 is difficult to interpret because [^{11}C]ABP688 is not in direct competition with glutamate, since they do not bind to the same site (Kew and Kemp, 2005). Due to changes in CGM V_T, our data suggest that the cerebellum may not be the most ideal reference region. In fact, in vitro saturation binding and autoradiography studies using mGluR5-specific compounds have reported

specific binding in the cerebellum of rhesus monkeys (Hamill et al., 2005; Patel et al., 2007). Thus, we cannot confidently interpret changes in BP_{ND} using the cerebellum as a reference region.

Limitations

Limitations of this study include a small $n = 3$ per group and large intersubject variability with [^{11}C]ABP688 mGluR5 binding, which made it difficult to observe any significant changes after NAC administration. As described above, our findings were consistent with other studies with [^{11}C]ABP688, where substantial intrasubject and intersubject variability has been found. Use of another mGluR5 tracer with lower variability, such as [^{18}F]F-PEB, would help address these limitations. A study in humans reported better test-retest reproducibility of BP_{ND} for [^{18}F]F-PEB than [^{11}C]ABP688 (Kuwabara et al., 2011). Smaller test-retest variation would permit the reliable detection of a pharmacological effect.

Changes in BP_{ND} were difficult to interpret due to increases in CGM V_T with the higher NAC dose as well as the test-retest increases. If residual ketamine is a contributing factor here, then, for future studies with [^{11}C]ABP688, the timing of ketamine between baseline and blocking tracer administration should be carefully controlled. Additional studies are needed to be certain that ketamine is not confounding baseline scans in the current single day, paired-bolus design. Finally, the glutamate system is complex and the interaction between pharmacological elevation in extrasynaptic glutamate levels and mGluR5 allosteric binding is not fully understood.

CONCLUSION

We failed to strictly replicate the results of Miyake et al., which reported a global reduction in [^{11}C]ABP688 binding after a NAC (50 mg/kg) challenge and no significant change from test to retest in baboons. Outcome measures for this study included V_T and BP_{ND}, where multiple kinetic modeling methods were used in the analysis. In rhesus monkeys, [^{11}C]ABP688 BP_{ND} was reduced in brain regions with both NAC doses (50 mg/kg and 100 mg/kg) but was not significantly different from baseline. V_T increased from baseline after both NAC doses, significantly at the 100 mg/kg NAC dose in multiple brain regions. Interpretability of BP_{ND} is difficult due to (1) test-retest BP_{ND} increases from morning to afternoon scans and (2) a significant increase in V_T at the 100 mg/kg NAC dose in the CGM reference region. High intersubject variability was observed within test-retest and baseline-NAC challenge groups, comparable with the baboon study. Although components of our study supported that of Miyake et al. when BP_{ND} was used, detecting alterations in glutamate at the metabotropic glutamate receptor subtype 5 should be conducted with a radiotracer with better test-retest reliability.

ACKNOWLEDGMENTS

The authors acknowledge the staff at the Yale PET Center, especially Krista Fowles and the NHP team, for conducting the PET experiments used in this study, and to Fei Liu, Ph.D., and Diana Martinez, M.D., of Columbia University for providing the reference standard and precursor for the synthesis and quality control of [^{11}C]ABP688. Special thanks go to Jenna Sullivan, Irina Esterlis, Evan Morris, and Gerard Sanacora for helpful scientific discussions.

REFERENCES

Ametamey SM, Kessler LJ, Honer M, Wyss MT, Buck A, Hintermann S, Auberson YP, Gasparini F, Schubiger PA. 2006. Radiosynthesis and preclinical evaluation of 11C-ABP688 as a probe for imaging the metabotropic glutamate receptor subtype 5. J Nucl Med 47:698–705.

Baker DA, Xi ZX, Shen H, Swanson CJ, Kalivas PW. 2002. The origin and neuronal function of in vivo nonsynaptic glutamate. J Neurosci 22:9134–9141.

Baker DA, Madayag A, Kristiansen LV, Meador-Woodruff JH, Haroutunian V, Raju I. 2008. Contribution of cystine-glutamate antiporters to the psychotomimetic effects of phencyclidine. Neuropsychopharmacology 33:1760–1772.

Carroll FI. 2008. Antagonists at metabotropic glutamate receptor subtype 5 structure activity relationships and therapeutic potential for addiction. Addict Rev 1141:221–232.

Carson RE, Channing MA, Blasberg RG, Dunn BB, Cohen RM, Rice KC, Herscovitch P. 1993. Comparison of bolus and infusion methods for receptor quantitation—Application to [F-18] cyclofoxy and positron emission tomography. J Cereb Blood Flow Metab 13:24–42.

Chen HH, Stoker A, Markou A. 2010. The glutamatergic compounds sarcosine and *N*-acetylcysteine ameliorate prepulse inhibition deficits in metabotropic glutamate 5 receptor knockout mice. Psychopharmacology 209:343–350.

Chowdhury GM, Behar KL, Cho W, Thomas MA, Rothman DL, Sanacora G. 2012. (1)H-[(1)(3)C]-nuclear magnetic resonance spectroscopy measures of ketamine's effect on amino acid neurotransmitter metabolism. Biol Psychiatry 71:1022–1025.

Cleva RM, Olive MF. 2011. Positive allosteric modulators of type 5 metabotropic glutamate receptors (mGluR5) and their therapeutic potential for the treatment of CNS disorders. Molecules 16:2097–2106.

Cleva RM, Gass JT, Widholm JJ, Olive MF. 2010. Glutamatergic targets for enhancing extinction learning in drug addiction. Curr Neuropharmacol 8:394–408.

Cosgrove KE, Galvan EJ, Barrionuevo G, Meriney SD. 2011. mGluRs modulate strength and timing of excitatory transmission in hippocampal area CA3. Mol Neurobiol 44:93–101.

Cunningham VJ, Rabiner EA, Slifstein M, Laruelle M, Gunn RN. 2010. Measuring drug occupancy in the absence of a reference region: The Lassen plot re-visited. J Cereb Blood Flow Metab 30:46–50.

de Bartolomeis A, Sarappa C, Magara S, Iasevoli F. 2012. Targeting glutamate system for novel antipsychotic approaches: relevance for residual psychotic symptoms and treatment resistant schizophrenia. Eur J Pharmacol 682:1–11.

Dean O, Giorlando F, Berk M. 2011. *N*-acetylcysteine in psychiatry: Current therapeutic evidence and potential mechanisms of action. J Psychiatry Neurosci 36:78–86.

Delforge J, Syrota A, Mazoyer BM. 1990. Identifiability analysis and parameter-identification of an in vivo ligand-receptor model from PET data. IEEE Trans Biomed Eng 37:653–661.

DeLorenzo C, Kumar JS, Mann JJ, Parsey RV. 2011a. In vivo variation in metabotropic glutamate receptor subtype 5 binding using positron emission tomography and [11C]ABP688. J Cereb Blood Flow Metab 31:2169–2180.

DeLorenzo C, Milak MS, Brennan KG, Kumar JS, Mann JJ, Parsey RV. 2011b. In vivo positron emission tomography imaging with

[(1)(1)C]ABP688: Binding variability and specificity for the metabotropic glutamate receptor subtype 5 in baboons. Eur J Nucl Med Mol Imaging 38:1083–1094.

Deschwanden A, Karolewicz B, Feyissa AM, Treyer V, Ametamey SM, Johayem A, Burger C, Auberson YP, Sovago J, Stockmeier CA, Buck A, Hasler G. 2011. Reduced metabotropic glutamate receptor 5 density in major depression determined by [(11)C]ABP688 PET and postmortem study. Am J Psychiatry 168:727–734.

Dodd S, Dean O, Copolov DL, Malhi GS, Berk M. 2008. *N*-acetylcysteine for antioxidant therapy: Pharmacology and clinical utility. Expert Opin Biol Ther 8:1955–1962.

Elmenhorst D, Minuzzi L, Aliaga A, Rowley J, Massarweh G, Diksic M, Bauer A, Rosa-Neto P. 2010. In vivo and in vitro validation of reference tissue models for the mGluR(5) ligand [(11)C]ABP688. J Cereb Blood Flow Metab 30:1538–1549.

Gunn RN, Gunn SR, Cunningham VJ. 2001. Positron emission tomography compartmental models. J Cereb Blood Flow Metab 21:635–652.

Gunn RN, Summerfield SG, Salinas CA, Read KD, Guo Q, Searle GE, Parker CA, Jeffrey P, Laruelle M. 2012. Combining PET biodistribution and equilibrium dialysis assays to assess the free brain concentration and BBB transport of CNS drugs. J Cereb Blood Flow Metab 32:874–883.

Hamill TG, Krause S, Ryan C, Bonnefous C, Govek S, Seiders TJ, Cosford ND, Roppe J, Kamenecka T, Patel S, Gibson RE, Sanabria S, Riffel K, Eng W, King C, Yang X, Green MD, O'Malley SS, Hargreaves R, Burns HD. 2005. Synthesis, characterization, and first successful monkey imaging studies of metabotropic glutamate receptor subtype 5 (mGluR5) PET radiotracers. Synapse 56:205–216.

Hilton J, Yokoi F, Dannals RF, Ravert HT, Szabo Z, Wong DF. 2000. Column-switching HPLC for the analysis of plasma in PET imaging studies. Nucl Med Biol 27:627–630.

Hintermann S, Vranesic I, Allgeier H, Brulisauer A, Hoyer D, Lemaire M, Moenius T, Urwyler S, Whitebread S, Gasparini F, Auberson YP. 2007. ABP688, a novel selective and high affinity ligand for the labeling of mGlu5 receptors: Identification, in vitro pharmacology, pharmacokinetic and biodistribution studies. Bioorg Med Chem 15:903–914.

Ichise M, Toyama H, Innis RB, Carson RE. 2002. Strategies to improve neuroreceptor parameter estimation by linear regression analysis. J Cereb Blood Flow Metab 22:1271–1281.

Innis RB, Cunningham VJ, Delforge J, Fujita M, Gjedde A, Gunn RN, Holden J, Houle S, Huang SC, Ichise M, Iida H, Ito H, Kimura Y, Koeppe RA, Knudsen GM, Knuuti J, Lammertsma AA, Laruelle M, Logan J, Maguire RP, Mintun MA, Morris ED, Parsey R, Price JC, Slifstein M, Sossi V, Suhara T, Votaw JR, Wong DF, Carson RE. 2007. Consensus nomenclature for in vivo imaging of reversibly binding radioligands. J Cereb Blood Flow Metab 27:1533–1539.

Kew JN, Kemp JA. 2005. Ionotropic and metabotropic glutamate receptor structure and pharmacology. Psychopharmacology 179:4–29.

Kuwabara K, Chamroonrat W, Mathews W, Waterhouse D, Brasic J, Guevara MR, Kumar A, Hamill T, Mozley PD, Wong DF. 2011. Evaluation of 11C-ABP688 and 18F-FPEB for imaging mGluR5 receptors in the human brain. J Nucl Med 52 (Suppl 1):390.

Lammertsma AA, Hume SP. 1996. Simplified reference tissue model for PET receptor studies. NeuroImage 4:153–158.

Laruelle M. 2000. Imaging synaptic neurotransmission with in vivo binding competition techniques: A critical review. J Cereb Blood Flow Metab 20:423–451.

Liu CY, Jiang XX, Zhu YH, Wei DN. 2012. Metabotropic glutamate receptor 5 antagonist 2-methyl-6-(phenylethynyl)pyridine produces antidepressant effects in rats: Role of brain-derived neurotrophic factor. Neuroscience 223C:219–224.

Michalon A, Sidorov M, Ballard TM, Ozmen L, Spooren W, Wettstein JG, Jaeschke G, Bear MF, Lindemann L. 2012. Chronic pharmacological mGlu5 inhibition corrects fragile X in adult mice. Neuron 74:49–56.

Miyake N, Skinbjerg M, Easwaramoorthy, B, Kumar D, Girgis RR, Xu X, Slifstein M, Abi-Dargham A. 2011. Imaging changes in glutamate transmission in vivo with the metabotropic glutamate receptor 5 tracer [11C] ABP688 and *N*-acetylcysteine challenge. Biol Psychiatry 69:822–824.

Moghaddam B, Adams B, Verma A, Daly D. 1997. Activation of glutamatergic neurotransmission by ketamine: a novel step in the pathway from NMDA receptor blockade to dopaminergic and cognitive disruptions associated with the prefrontal cortex. J Neurosci 17:2921–2927.

O'Brien JA, Lemaire W, Chen TB, Chang RS, Jacobson MA, Ha SN, Lindsley CW, Schaffhauser HJ, Sur C, Pettibone DJ, Conn PJ, Williams DL Jr. 2003. A family of highly selective allosteric modulators of the metabotropic glutamate receptor subtype 5. Mol Pharmacol 64:731–740.

Pajevic S, Daube-Witherspoon ME, Bacharach SL, Carson RE. 1998. Noise characteristics of 3-D and 2-D PET images. IEEE Trans Med Imaging 17:9–23.

Patel S, Hamill TG, Connolly B, Jagoda E, Li W, Gibson RE. 2007. Species differences in mGluR5 binding sites in mammalian central nervous system determined using in vitro binding with [18F]F-PEB. Nucl Med Biol 34:1009–1017.

Perroy J, Raynaud F, Homburger V, Rousset MC, Telley L, Bockaert J, Fagni L. 2008. Direct interaction enables cross-talk between ionotropic and group I metabotropic glutamate receptors. J Biol Chem 283:6799–6805.

Riaza Bermudo-Soriano C, Perez-Rodriguez MM, Vaquero-Lorenzo C, Baca-Garcia E. 2012. New perspectives in glutamate and anxiety. Pharmacol Biochem Behav 100:752–774.

Sandiego CM, Weinzimmer D, Carson RE. 2013. Optimization of PET-MR registrations for nonhuman primates using mutual information measures: A Multi-Transform Method (MTM). NeuroImage 64:571–581.

Shen LH, Liao MH, Tseng YC. 2012. Recent advances in imaging of dopaminergic neurons for evaluation of neuropsychiatric disorders. J Biomed Biotechnol 2012:259349.

Sokol DK, Maloney B, Long JM, Ray B, Lahiri DK. 2011. Autism, Alzheimer disease, and fragile X: APP, FMRP, and mGluR5 are molecular links. Neurology 76:1344–1352.

Spooren W, Ballard T, Gasparini F, Amalric M, Mutel V, Schreiber R. 2003. Insight into the function of Group I and Group II metabotropic glutamate (mGlu) receptors: behavioural characterization and implications for the treatment of CNS disorders. Behav Pharmacol 14:257–277.